第 31卷 第 3期　　　　焊 接 学 报　　　　Vol.31　No.3
2010年 3月　　TRANSACTIONS OF THE CHINA WELDING INSTITUTION　　March　2010

单相交流点焊电源功率因数的精确计算方法

张 勇，马铁军，贺有旭，杨思乾*
(西北工业大学 陕西省摩擦焊接重点实验室，西安 710072)

摘 要：借鉴电力系统关于非正弦电流电网功率因数的频域定义方法，考虑电流谐波分量和相位因素对有功功率的影响，应用快速傅立叶变换对电网电压和焊接电流信号进行频域分解，计算获得了准确的交流点焊电源功率因数．在交流点焊机上进行短路焊接试验时，采用文中提出的方法计算相应的功率因数．结果表明，改变点焊机二次回路臂长引起的功率因数变化规律与理论分析结果相符；相同控制角计算所得的功率因数值较传统 θ角法所得值小，与电力系统采用频域法对非正弦电流电网功率因数的计量结果一致．试验结果初步证明了提出的计算方法是可靠有效的．

关键词：交流点焊；功率因数；频谱分析
中图分类号：TG438.2　　文献标识码：A　　文章编号：0253－360X(2010)03－0085－04

张 勇

0 序 言

单相交流点焊电源由于主电路简单、控制电路成熟、操作方便、价格低廉，目前仍是电阻焊领域使用最为广泛的一种电源[1,2]．然而，交流点焊电源的功率因数会随着铁磁物焊件伸入二次回路的多少、电极臂长的变化以及焊接变压器功率级数的改变等因素发生变化，从而对焊接质量产生影响．因此，交流点焊电源功率因数的检测及实时补偿，一直是研究高精度单相交流点焊控制器重点关注的问题．西北工业大学吴禄教授等人[3]根据点焊电源数学模型，通过晶闸管控制角和实测的晶闸管导通角计算功率因数（简称 θ角法）；上海交通大学的贡亮等人[4]采用电流过零导数比法测量电阻焊动态功率因数；美国的 Dennis[5]通过检测动态电阻实现功率因数的补偿．

文中基于单相交流点焊焊接电流波形严重非正弦畸变、含有大量高次谐波的特点，对电网电压和焊接电流信号进行快速傅立叶变换，运用频域分解方法计算获得更为准确的功率因数，为进一步提高交流点焊电源控制系统水平奠定理论基础．

1 理论分析

众所周知，交流电阻点焊电源实质上是一个感性负载电源，焊接电流为非正弦畸变波形，其主电路等效电路及电压、电流波形如图 1所示．图 1a中，R，L分别为焊接变压器初级和次级回路的等效电阻和电感，K为等效电子开关．解图 1a电路的微分方程，可得图 1b[4]中阴影所示瞬时电流 i 的数学关系式为

$$i=\frac{\sqrt{2}U}{Z}\left[\sin(\omega t+\alpha-\varphi)-\sin(\alpha-\varphi)e^{-\frac{\omega t}{\tan\varphi}}\right]=i_1+i_2 \tag{1}$$

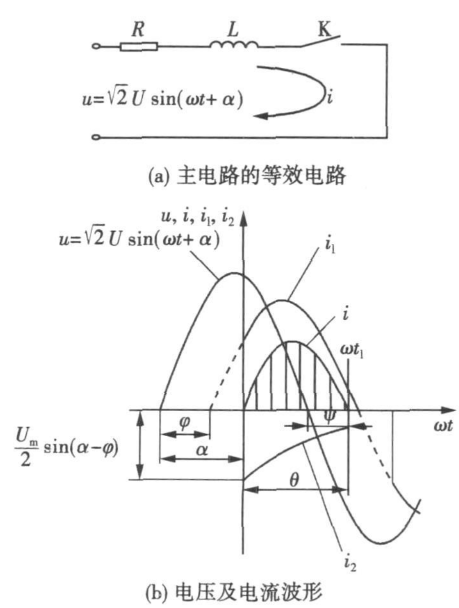

图 1 交流点焊电源主电路的等效电路及电压、电流波形
Fig. 1 Equivalent circuit, voltage and current waveforms of main circuit for AC spot welding power supply

收稿日期：2009－09－03
*参加此项研究工作的还有谢红霞，李 佳

式中：$Z=\sqrt{R^2+(\omega L)^2}$为回路等效阻抗（Ω）；$\varphi=\mathrm{tg}^{-1}(\omega L/R)$为回路功率因数角（rad）；ω为交流电压的角频率（rad/s）；U为网络电压的有效值（V）；α为晶闸管的控制角（rad）；i_1为稳态电流（A）；i_2为暂态电流（A）。

从图 1b可以看出，交流电阻点焊电源属于典型的非正弦周期电流负载，其功率因数角被湮没在网路电压与焊接电流的相位差中，无法直接提取[4]。在国际电工界和电力系统领域，研究非正弦条件下电网的电力参数的定义或计量的方法已有很长历史，提出了多种定义方法，其中得到普遍认可的是一种基于频域分解的方法[6,7]。该方法利用数学中正交函数的有关概念，将非正弦电流 $i(t)$分解为基波电流 $i_1(t)$和谐波电流 $i_h(t)$，即

$$i(t)=i_1(t)+i_h(t) \tag{2}$$

式中：$i_1(t)$与 $i_h(t)$正交。进一步将基波电流 $i_1(t)$分解为与正弦电压同相的有功电流 $i_p(t)$和与其正交的无功电流 $i_q(t)$，即

$$i_1(t)=i_p(t)+i_q(t) \tag{3}$$

在此基础上，定义与有功、无功、谐波电流对应的有功、无功和畸变（虚功）功率。而视在功率则由有功功率、无功功率和畸变功率三项组成。因此，在非正弦电流情况下，根据产生有功功率、无功功率和畸变功率的电流相互正交的特点，正确可行的电网功率因数计算方法为

$$\cos\varphi=\frac{P}{S}=\frac{P}{UI} \tag{4}$$

式中：P为有功功率（W）；S为视在功率（VA）；U为电压有效值（V）；I为电流有效值（A）。

2 交流点焊电源功率因数的频域分解计算

图 2、图 3是通过频谱分析得到的交流点焊焊接电流和电网电压波形的幅频图，图中纵坐标为与原始信号的峰值和采样点数有关的幅度相对量。由图 2可见，交流点焊焊接电流主要由奇次谐波分量构成，且 3次谐波（150 Hz）和 5次谐波（250 Hz）幅值较高。

在频域分解方法中，频域功率定义的本质是将各次谐波的功率值相加作为总的功率值，而只有与正弦电压同相的有功电流才产生有功功率，因为谐波电流和无功电流会使电网电流增加、占用电网系统容量、产生高频加热损失等[6,8]。但在点焊焊接过程中，并不是只有基波电流才为点焊提供所需的焦

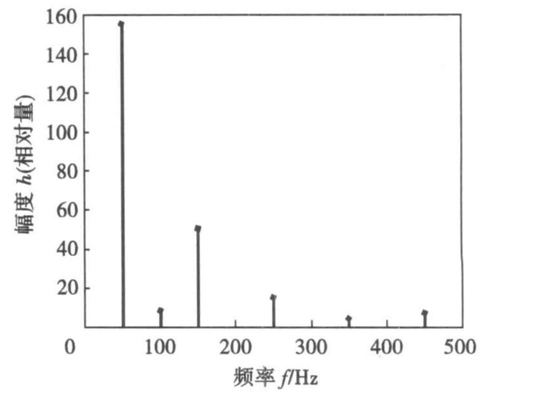

图 2 交流点焊焊接电流幅频

Fig. 2 Amplitude-frequency charts of AC spot welding current waveforms

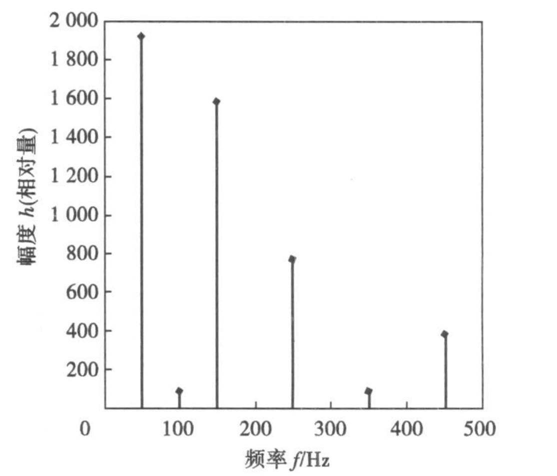

图 3 电网电压幅频

Fig. 3 Amplitude-frequency charts of grid voltage

耳热，其余的谐波分量，特别是 3次谐波对点焊提供的焦耳热也不容忽视。在应用频域分解方法计算点焊电源的功率因数时，应当与电力系统计量电网功率因数的方法有所区别，谐波分量在增加电网电流的同时，也为点焊提供了有用的焦耳热。因此，从点焊电源角度及其加热特点出发，功率因数应当考虑点焊电流波形的谐波分量及相位因素对有功功率的贡献和影响。

设交流点焊电源的网路电压为 u，焊接电流为 i，则通过傅立叶级数，电压和电流分别为

$$u=U_0+\sum_{k=1}^{\infty}U_{mk}\sin(k\omega t+\varphi_{uk}) \tag{5}$$

$$i=I_0+\sum_{k=1}^{\infty}I_{mk}\sin(k\omega t+\varphi_{ik}) \tag{6}$$

式中：k为正整数；U_0为电压的直流分量（V）；I_0为电流的直流分量（A）；U_{mk}，φ_{uk}分别对应电压各次正弦分量的振幅（V）和初相（rad）；I_{mk}，φ_{ik}分别对应电

流各次正弦分量的振幅(A)和初相(rad).

考虑谐波分量及相位因素对有功功率的贡献和影响,并且考虑当波形不对称时还将含有直流分量,可得交流点焊电源的有功功率和视在功率为

$$P = U_0 I_0 + \sum_{k=1}^{\infty} U_k I_k \cos(\varphi_{uk} - \varphi_{ik}) \tag{7}$$

$$S = UI = \sqrt{U_0^2 + U_1^2 + U_2^2 + \cdots} \times \sqrt{I_0^2 + I_1^2 + I_2^2 + \cdots} \tag{8}$$

借鉴电力系统频域分解方法对功率因数的定义,可得交流点焊电源的功率因数为

$$\cos\varphi = \frac{P}{S} = \frac{P}{UI} \tag{9}$$

计算过程中,首先对点焊焊接电流及网路电压波形进行采样,再将采样信号进行快速傅立叶变换,并做出其幅频图和相频图,随后选择频谱图中基波、高次谐波数据和合适的 k值,将式(7)、式(8)计算结果代入式(9),即可得到准确的功率因数值.

从图 2、图 3可以看出,5次以后的各谐波分量的幅值已经非常小,故仅需计算基波和 3次、5次谐波幅值,即可得到较高的计算精度,且可有利于焊接过程的实时控制.

3 功率因数计算的验证

3.1 试验测试分析系统及验证方法

采用西北工业大学研制的 KD(T)—4型单片机点焊控制箱,控制 NA—200—4型交流点焊机进行验证试验.测试分析系统如图 4所示,在点焊焊接过程中,使用 TDS2014B型数字存储示波器,经过单片机控制箱内的前置处理电路获得焊接电流、电网电压信号的采样波形,并由示波器将波形数据送入计算机进行频谱分析,随后按照上述方法计算功率因数.焊接过程各周波晶闸管的控制角、导通角等均由单片机控制系统测量并存储,焊接结束后可读出相应数据.

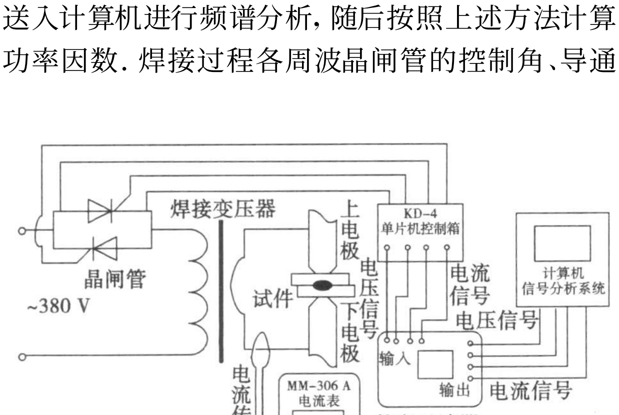

图 4 焊接电流及电网电压测试分析系统示意图

Fig. 4 Block diagram of testing system for welding current and grid voltage

为了验证提出的功率因数计算方法的有效性,首先在短路焊接时保持晶闸管控制角不变的条件下,通过改变点焊机二次回路机臂长度,测量计算得到一组功率因数值,然后保持点焊机二次回路机臂长度不变,在短路焊接时,改变晶闸管的控制角,测量、计算得到一组功率因数值,并与 θ角法所得的功率因数值比较.

3.2 测试结果分析

图 5是在焊接变压器为 10级、热量百分数为 55%、通电时间为 15周波的条件下,点焊机二次回路机臂长度从 510~610 mm变化,试验所得到的功率因数与点焊机二次回路机臂长度的关系曲线.由图 5可以看出,随着电极臂长的增大,功率因数呈单调下降的趋势.如图 1a点焊机主电路的等效电路所示,当电极臂增长时,点焊机二次回路所包围的面积将随之增大,引起等效电感和感抗的相应增大,根据阻抗三角形的变化规律可知,此时功率因数角 φ将增大,即功率因数 cosφ变小.由此可见,试验所得功率因数与臂长的变化规律同理论分析结果相符.

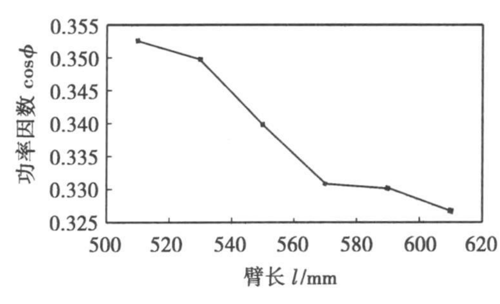

图 5 功率因数与臂长的关系

Fig. 5 Relationship between power factor and electrode arm length

表 1是在点焊机二次回路机臂长度为 590 mm,焊接变压器为 10级、通电时间为 15周波的条件下,改变热量百分数,即改变晶闸管的控制角,短路焊接时采用文中方法(频域法)得到的功率因数值,以及相同条件同一次焊接过程,利用传统 θ角法所得的功率因数值.

由表 1可见,在晶闸管的控制角为 127.8°电角度时,实测 θ角为 77.7°电角度,此时利用传统 θ角法所得的功率因数值与采用文中的频域法所得的功率因数值偏差达到 0.554,随着控制角的减小,晶闸管的导通角增大,两种算法所得功率因数值的偏差减小.实际中,当晶闸管导通角很小时,由于电流波

表 1 θ角法和频域法所得功率因数值的比较
Table 1 Comparison of power factor values calculated by θ method and frequency-domain method

控制角 α/(°)	实测 θ/(°)	θ角法 功率因数角 φ_1/(°)	θ角法 功率因数 $\cos\varphi_1$	频域法 功率因数角 φ_2/(°)	频域法 功率因数 $\cos\varphi_2$	功率因数偏差
127.8	77.7	32.05	0.848	72.90	0.294	0.554
124.2	85.2	37.95	0.789	74.50	0.267	0.522
119.7	94.6	45.08	0.706	73.47	0.285	0.421
114.3	102.7	47.11	0.681	72.72	0.297	0.384
109.8	110.9	50.92	0.630	72.22	0.305	0.325
106.2	116.8	52.81	0.604	71.68	0.314	0.290
102.6	120.8	51.72	0.620	71.21	0.322	0.298
98.1	128.7	55.05	0.573	71.08	0.324	0.249
92.7	134.0	53.01	0.602	69.48	0.351	0.251
88.2	142.9	56.95	0.545	69.87	0.344	0.201
84.6	148.3	58.05	0.529	70.42	0.335	0.194

形畸变严重,其谐波和相位因素对功率因数的影响加剧,造成两种算法所得的功率因数值偏差较大;随着晶闸管导通角的增大,电流波形畸变减小,更接近于理想的正弦波,此时两种算法所得的功率因数值偏差就小. 另一方面,θ角法由于是依据与电流峰值之间的经验关系来进行控制的,且由于测量电路存在的误差,故其精度与频域法有一定差距。

在文献[7]中,应用传统的计量方法和采用频域计量法分别对非正弦电流电网的功率因数进行了测量,结果发现,前者所得的功率因数值高出实际值0.3左右. 表 1中,当控制角在 100°电角度左右即晶闸管导通角在 115°电角度附近时,θ角法和频域法所得的功率因数值偏差也在 0.3左右,说明试验结果与电力系统对非正弦电流电网功率因数的测量结果基本吻合,从而初步证明了提出的点焊电源功率因数计算方法的有效性.

4 结 论

(1)以非正弦电流电网功率因数的频域计量研究理论为基础,结合交流点焊电源的加热特点,提出了一种基于频谱分析、考虑高次谐波计算交流点焊电源功率因数的方法.

(2)随着交流点焊机二次电极臂长的增大,运用文中提出的方法计算所得的功率因数呈单调下降的变化规律,与理论分析相符;相同控制角,运用文中提出的频域法计算所得的功率因数值,较传统θ角法所得值小,与电力系统采用频域法对非正弦电流电网功率因数的计量结果一致. 试验结果初步证明了文中提出的计算交流点焊电源功率因数的方法是可靠有效的.

参考文献:

[1] 王 清, 吴 林, 张相军, 等. 不断发展与完善之中的电阻焊焊接电源[J]. 焊接, 2000(3): 7-10.
Wang Qing, Wu Lin, Zhang Xiangjun, et al. Resistance welding machine in developing and perfecting[J]. Welding & Joining, 2000(3): 7-10.

[2] Cho Yongjoon, Rhee Sehun. Primary circuit dynamic resistance monitoring and its application to quality estimation during resistance spot welding[J]. Welding Journal, 2002(6): 104s-111s.

[3] 吴 禄, 黎康保, 赵亚光. 关于应用微处理机检测点焊焊接电流有效值的研究[J]. 焊接学报, 1985, 6(1): 31-37.
Wu Lu, Li Kangbao, Zhao Yaguang. Detection of spot welding current RMS using microprocessor[J]. Transactions of the China Welding Institution, 1985, 6(1): 31-37.

[4] 贡 亮, 刘成良. 交流电阻焊动态功率因数的实时解析算法[J]. 上海交通大学学报, 2006, 40(6): 884-888.
Gong Liang, Liu Chengliang. The analytic algorithm for real-time calculating the dynamic power factor in AC resistance welding[J]. Journal of Shanghai Jiaotong University, 2006, 40(6): 884-888.

[5] Dennis J. Power factor monitoring and control system for resistance welding[J]. Welding Journal, 1987, 66(2): 24-28.

[6] 王 群, 刘进军, 王兆安. 非正弦周期电流的频域和时域分解方法[J]. 电力系统自动化, 2000(1): 21-25.
Wang Qun, Liu Jinjun, Wang Zhaoan. Decompostion approaches in frequency-domain and time-domain for non-sinusoidal periodic current[J]. Power Systems Automation, 2000(1): 21-25.

[7] 刘学会, 张 伟, 王永刚, 等. 非正弦电流电网的功率因数及其测量[J]. 电测与仪表, 2004, 41(1): 23-25.
Liu Xuehui, Zhang Wei, Wang Yonggang, et al. The power factor and its measurement of non-sinusoidal AC electric network[J]. Electrical Measurement & Instrumentation, 2004, 41(1): 23-25.

[8] 王学伟, 高 朝. 畸变波形下功率定义问题的探讨[J]. 电网技术, 2004, 28(23): 17-21.
Wang Xuewei, Gao Zhao. A research on power definition under distored wave[J]. Power System Technology, 2004, 28(23): 17-21.

作者简介: 张 勇, 男, 1965年出生, 博士, 副教授. 主要从事电阻焊理论与质量控制方面的教学和科研工作. 发表论文 20余篇.
Email: hjzhyong@nwpu.edu.cn

that the ductile fracture characteristics when the content of In exceeded 2%, the dissociation morphology fracture would be emerged which had little influence on the tensile property of the brazed joints. The elements of Ga and In distributed uniformly, no segregation in the microstructure of the Ag-Cu-Zn-Sn-3Ga-2In filler metal was observed by SEM, and the significant framework structure was found in the matrix.

Key words: Ag based brazing filler metal; microstructure; Ga; In

Prediction of tensile property of TIG welding joints in GH99 alloy by artificial neural network

WANG Qing, NA Yue, SUN Dongli, LIU Yuhong, DENG Dejun, YANG Yuyin (1. School of Materials Science and Engineering, Harbin Institute of Technology, Harbin 150001, China; 2. Beijing Power Generating Machinery Institute, Beijing 100072, China). p 77—80

Abstract: Multilayer BP network model based on improved algorithm was established with Matlab 7.0 software to predict the tensile property of TIG welding joints of GH99 superalloy. The input parameters of the model consisted welding current, welding speed, pulse frequency, remelting times, plate thickness, assembly clearance and weld groove. The outputs of the Artificial Neural Network (ANN) model included property parameters, such as tensile strength, yield strength and elongation. The calculated results showed that the multilayer BP network model based on improved algorithm could predict the tensile property of TIG welding joints of GH99 superalloy. The calculated values were in good agreement with measured data, and the average relative errors between calculated values and measured data of tensile strength, yield strength and elongation were -0.76%, 1.71% and 2.30%, respectively.

Key words: GH99 alloy; TIG welding; artificial neural network; tensile property

Evaporation loss of Mg element in pulsed laser welding of 5A05 aluminum alloy and distribution of micro-hardness of welding joint

NIU Ruifeng, LIN Binghua, WANG Yani, YANG Xingfei (School of Materials Science and Engineering, Xi'an University of Technology, Xi'an 710048, China). p 81—84

Abstract: 5A05 aluminum alloy plate with the thickness of 1 mm was welded with Nd: YAG laser beam. The effect of welding parameters including pulse energy, pulse duration, welding speed and defocusing distance on the evaporation loss of Mg element, depth of fusion, variation of Mg element content in weld metal and micro-hardness of weld-joint were studied and analyzed. The results showed that stirring in molten pool had a significant effect on the evaporation loss of Mg element. With the increase of stirring and the weld penetration, the evaporation loss of Mg element was decreased. Due to the effect of Mg element content and cooling rate, the maximum hardness of weld joint was approximately located at the fusion line. From the surface to the bottom of molten pool, the hardness of weld joint first decrease and then increase.

Key words: pulsed Nd: YAG laser welding; evaporation loss of Mg element; aluminum alloy; micro-hardness

Precise calculation methods of power factor for single-phase alternating current spot welding machine

ZHANG Yong, MA Tiejun, HE Youxu, YANG Sijian (Shanxi Key Laboratory of Friction Welding Technologies, Northwestern Polytechnical University, Xi'an 710072, China). p 85—88

Abstract: Collaborating with the definition of the power factor for the non-sinusoidal waveform, this paper adopted the Fast Fourier Transformation (FFT) to analyze the spectrum of grid voltage and welding current, considered the influence of current harmonics and their phase shifts on the active power, eventually calculated and obtained the accurate power factor of an alternative current spot welding machine. The results showed good coincidence with the theoretical analysis when the power factor changed with the length of the secondary loop. With the same triggering angle of the silicon-controlled rectifier (SCR), the calculated power factor was smaller than that obtained by the traditional angle θ method, but was identical with the data which was measured by the power system. In conclusion, the proposed method is feasible and effective.

Key words: alternating current spot welding; power factor; frequency-domain analysis

Mechanical and fatigue properties of undermatching butt joints of 10CrNi3MoV steel

ZHAO Zhili, YANG Jianguo, LIU Xuesong, FANG Hongyuan (1. School of Materials Science & Engineering, Harbin University of Science and Technology, Harbin 150040, China; 2. State Key Laboratory of Advanced Welding Production Technology, Harbin Institute of Technology, Harbin 150001, China). p 89—92

Abstract: Based on the tension and pulse fatigue tests, the influence of mismatch ratio on mechanical performance of undermatching flush butt joints of 10CrNi3MoV steel was studied, and the empirical equations for the relationship between mismatch ratio and fatigue strength (or fatigue life) of joints were built. The results of experiments illustrated that the tensile strength, specific elongation and fatigue strength of flushing butt joints decreased with the decreasing mismatch ratio, and the influence on specific elongation and fatigue strength was obviously higher than that on the tensile strength. The tensile strength and fatigue strength of undermatching flush butt joints exceed their deposited metals by the metallurgic strengthening effect and constrained strength effect on weld metal. Because a low to excess of mismatch ratio welded structure lacking plasticity reserve of need, the preliminary definition of low limit of mismatch ratio was attempted under standard of the rupture models of welded joints.

Key words: undermatching butt joints; mechanical properties; fatigue properties; mismatch ratio

Mechanism of cracks generation in hardfacing pinch roll

WANG Qingbao[1,2], LI Zhuoxin[1], SHI Yaowu[1] (1. Department of Materials Science and Engineering, Beijing University of Technology, Beijing 100022, China; 2. MCC Welding Science & Technology Co. Ltd., Beijing 100088, China). p 93—96

Abstract: Hot cracks formed in pinch roll frequently after repaired by hardfacing because the material was chosen improperly and low purity. This happened even if the hardfacing tech-